Optical properties of soda lime float glass from 3 mm to 148 nm (0.41 meV to 8.38 eV) by spectroscopic ellipsometry

Maxwell M. Junda and Nikolas J. Podraza[a)]

Department of Physics & Astronomy and The Wright Center for Photovoltaics Innovation & Commercialization, University of Toledo, Toledo, OH 43606, USA

[a)] Electronic mail: Nikolas.Podraza@utoledo.edu

The optical properties of soda lime float glass (SLG) have been characterized over a wide spectral range from 0.41 meV – 8.38 eV using spectroscopic ellipsometry and from 0.74 – 4.80 eV by unpolarized transmittance spectroscopy to retain sensitivity to the onset of high photon energy absorption. In all, the raw measured spectra are collected using four separate instruments, each covering different portions of the full measured spectrum. The glass is modeled as two separate surface layers on either side of a bulk SLG slab to account for variations in surface properties arising from the float glass fabrication process. The measurements are sensitive to the thicknesses of each of these layers and to the optical properties of each, which are reported as both the complex dielectric function ($\varepsilon = \varepsilon_1 + i\varepsilon_2$) and complex index of refraction ($N = n + ik$). Despite the measurements being collected on multiple instruments, the optical properties of each layer are represented as single, continuous parametric functions.

INTRODUCTION

Soda lime float glass (SLG) is a ubiquitous planar glass that is used in a wide variety of applications. The production process involves cooling a molten layer of glass floating upon a denser molten layer of tin such that the glass layer solidifies upon the tin which remains liquid. The planar sheet of SLG has two optically distinct surfaces resulting from this process. The

surface that was in contact with the tin, hereafter referred to the "tin side," has a surface layer whose properties differ from that of the bulk SLG as a result of tin diffusion into the glass. The other side, hereafter referred to as the "air side," was only exposed to the production environment ambient and has a surface layer with properties more similar to those of the underlying bulk SLG.

In this work, a single piece of SLG is optically characterized by wide spectral range spectroscopic ellipsometry (SE) from 0.41 meV – 8.37 eV and by unpolarized transmittance spectroscopy from 0.74 – 4.80 eV. These measurements are used to determine the thickness of the air side, tin side, and bulk glass layers as well as their associated spectroscopic optical response functions in the form of the complex dielectric function ($\varepsilon = \varepsilon_1 + i\varepsilon_2$) and complex index of refraction ($N = n + ik$).

SSS Journal Banner

Accession #:	01425
Technique:	SE
Host Material:	air ambient/soda lime glass/air ambient
Instrument:	J. A. Woollam Co., Inc. VUV-VASE, J. A. Woollam Co., Inc. M-2000FI, J. A. Woollam Co., Inc. IR-VASE, J. A. Woollam Co., Inc. THz-VASE
Published Spectra:	4
Spectra in Electronic Record:	4
Published Figures:	7
Spectral Category:	Technical

SPECIMEN DESCRIPTION

Specimen Number:	1 of 1
Bulk Material:	air ambient/soda lime glass/air ambient
Specimen Temperature During Analysis:	295 K (Room Temperature)
Sample Conditions During Measurement:	Air

FIG. 1. Depiction of specimen layers.	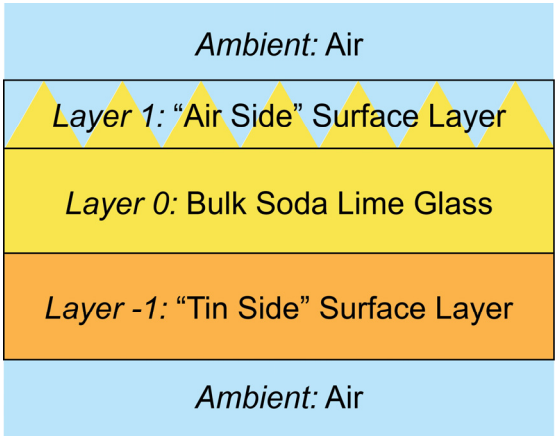

SPECIMEN COMPONENT LAYERS

■ *Layer 0*

Layer Composition/Structure:	Soda Lime Glass
CAS Registry No:	
Layer Manufacturer/Supplier:	Pilkington NSG
Host Material Characteristics:	solid, homogeneous, amorphous, insulator, glass
Chemical Name:	N/A
Layer Composition:	SiO_2, Na_2O, CaO, MgO, Al_2O_3, K_2O, SO_3, Fe_2O_3 (See Ref. 1)
Layer Form:	
Lot Number:	N/A
Structural Formula:	amorphous
Analyzed Region:	surface
***Ex Situ* Preparation/Mounting:**	Methanol wipe
***In Situ* Preparation:**	N/A
Specimen Temperature During Analysis, K:	295 K
Maximum Chamber Pressure During Analysis, Pa:	N/A

INSTRUMENT CONFIGURATION

Instrument #	1 of 4
Instrument Manufacturer:	J. A. Woollam Co., Inc
Manufacturer Model No:	VUV-VASE
Instrument Configuration:	Rotating analyzer N_2 purged spectroscopic ellipsometer operated with adjustable retarder present in beam path
Spectral Range:	210 – 145 nm (5.90 – 8.37 eV)
Measurement Angle(s) of Incidence:	50°
Acquired Data Type:	$N = \cos(2\psi)$, $C = \sin(2\psi)\cos\Delta$, $S = \sin(2\psi)\sin\Delta$

Instrument #	2 of 4
Instrument Manufacturer:	J. A. Woollam Co., Inc
Manufacturer Model No:	M-2000FI
Instrument Configuration:	multichannel, rotating compensator spectroscopic ellipsometer
Spectral Range:	1688 – 211 nm (0.73 – 5.89 eV)
Measurement Angle(s) of Incidence:	50° (SE), 0° (Transmittance)
Acquired Data Type:	$N = \cos(2\psi)$, $C = \sin(2\psi)\cos\Delta$, $S = \sin(2\psi)\sin\Delta$; unpolarized transmittance

Instrument #	3 of 4
Instrument Manufacturer:	J. A. Woollam Co., Inc
Manufacturer Model No:	IR-VASE
Instrument Configuration:	Fourier transform, rotating compensator spectroscopic ellipsometer
Spectral Range:	24.78 – 1.70 μm (0.05 – 0.73 eV)
Measurement Angle(s) of Incidence:	50°
Acquired Data Type:	$N = \cos(2\psi)$, $C = \sin(2\psi)\cos\Delta$, $S = \sin(2\psi)\sin\Delta$

Instrument #	4 of 4
Instrument Manufacturer:	J. A. Woollam Co., Inc
Manufacturer Model No:	THz-VASE
Instrument Configuration:	Single channel, simultaneously rotating polarizer and rotating compensator spectroscopic ellipsometer
Spectral Range:	3.00 – 0.31 mm (0.41 – 3.97 meV)
Measurement Angle(s) of Incidence:	50°
Acquired Data Type:	$N = \cos(2\psi)$, $C = \sin(2\psi)\cos\Delta$, $S = \sin(2\psi)\sin\Delta$

DATA ANALYSIS

The optical properties in the form of the complex dielectric function ($\varepsilon = \varepsilon_1 + i\varepsilon_2$) and structural properties in the form of layer thicknesses are determined by fitting parameterized, layered models to the measured spectra. The fitting is accomplished using an iterative least squares regression algorithm to minimize an unweighted error function σ that quantifies the difference between model-simulated and measured spectra[2]. The sensitivity to different layers of the sample varies depending on the wavelength of the probing light and the measurement configuration. Consequently, the wide spectral range measurements presented here are best analyzed by disassembling the full spectrum so that each spectral portion can be fit by an appropriate structural model containing only layers to which the constituent wavelengths are sensitive. Each of these models are fit simultaneously with a single set of optical properties of each layer being held common across all structural models and data sets. Thus, this modeling configuration is capable of handling the differences in optical effects arising at vastly different wavelengths while determining a single, continuous ε describing the optical response of each layer. Each model is composed of some or all layers shown in Figure 1 as appropriate for the wavelengths being modeled. In particular, both sides of the specimen are measured from 0.05 – 8.37 eV using reflection-mode SE which has sufficient surface sensitivity to characterize the air side and tin side layers as well as the bulk SLG layer. Due to the long wavelengths of probing light and relatively thin surface layer thicknesses, the reflection SE measurements in the THz

(0.41 - 3.97 meV) spectral range are not sensitive to the presence of either the air or tin side surface layers so only a single measurement is analyzed. Finally, the unpolarized transmittance measurement collected from 0.74 – 4.80 eV is sensitive to weak absorption arising in all layers and is therefore modeled using all layers. The specific configurations of each model and associated spectral range are shown schematically in Figure 2. Parametric ε describing the bulk SLG layer is described as the sum of Sellmeier[3], Gaussian[4,5], and Tauc-Lorentz[6,7] oscillators whereas the tin side surface layer is described as the sum of Sellmeier[3], Gaussian[4,5], and Lorentz[3] oscillators. A constant additive term to the real part of ε, ε_1, equal to unity is included in the parameterizations for both the tin side surface and bulk SLG. Spectra in ε representing the air side surface roughness layer of the glass is described as a Bruggeman effective medium

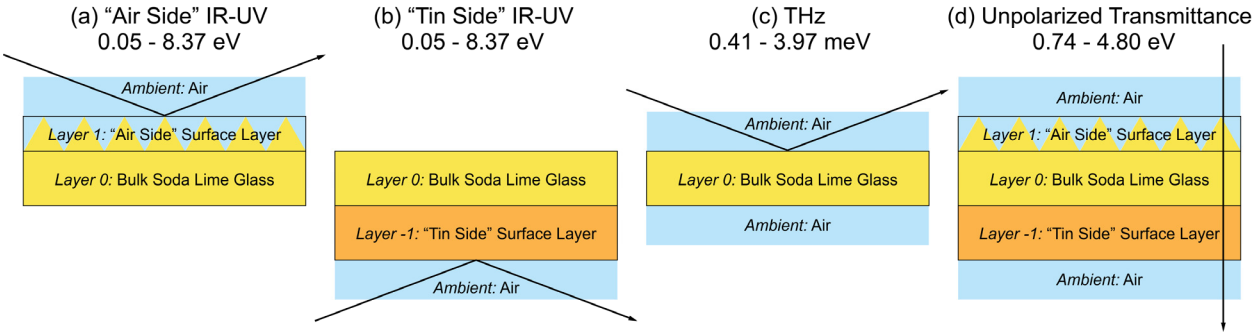

FIG. 2. Schematics of the layered structural models simultaneously fit to all measured ellipsometric and transmittance spectra. Each model includes only layers to which the associated probing wavelengths and measurement type (ellipsometric, transmittance) are sensitive. Any layers appearing in multiple models are described by a common, continuous optical response function. The black arrows indicate the direction and configuration (i.e. reflection or transmission) of the measurement beam (Accession #01425).

approximation[8,9] (EMA) with 0.5 volume fraction identical to the bulk SLG and the other 0.5 volume fraction consisting of void, in accordance with previously published modeling procedures for SLG[10]. Both the void in the air side EMA and the air ambient on either side of the glass are described by $\varepsilon = 1$. Finally, after the aforementioned parametric models are fit, all optical and structural parameters are fixed and a numerical inversion fitting procedure[11] is applied as an alternative technique for obtaining the ε describing the bulk SLG layer. The inversion is able to more effectively resolve the low amplitude features present in the highly sensitive transmittance measurements.

Figure 3(a)-(c) shows all measured $N = \cos(2\psi)$, $C = \sin(2\psi)\cos\Delta$, $S = \sin(2\psi)\sin\Delta$ spectra and the associated model fits that are generated from the schematics shown in Figure 2.

Figure 3(d) shows the measured transmittance spectrum and the model fits obtained both with fully parametric ε and with an inverted SLG bulk layer ε. Despite the fact that multiple models are used, the fitting is simultaneous such that the parametric results shown in Figure 3 are described by a single error function $\sigma = 0.03437$. The model simulations shown in panels (a) – (d) in Figure 3 correspond to the models shown as (a) – (d) in Figure 2, respectively. Figure 4 shows ε describing the bulk SLG layer over the full measured spectral range. Spectral regions outside the measured ranges are extrapolated from the parametric equations describing ε and are shown in gray. Additionally, low amplitude ε_2 obtained from numerical inversion of the transmittance spectra is shown in the inset as red points. ε describing the optical response of the tin side layer is shown in Figure 5. It should be noted that the optical response for the tin side

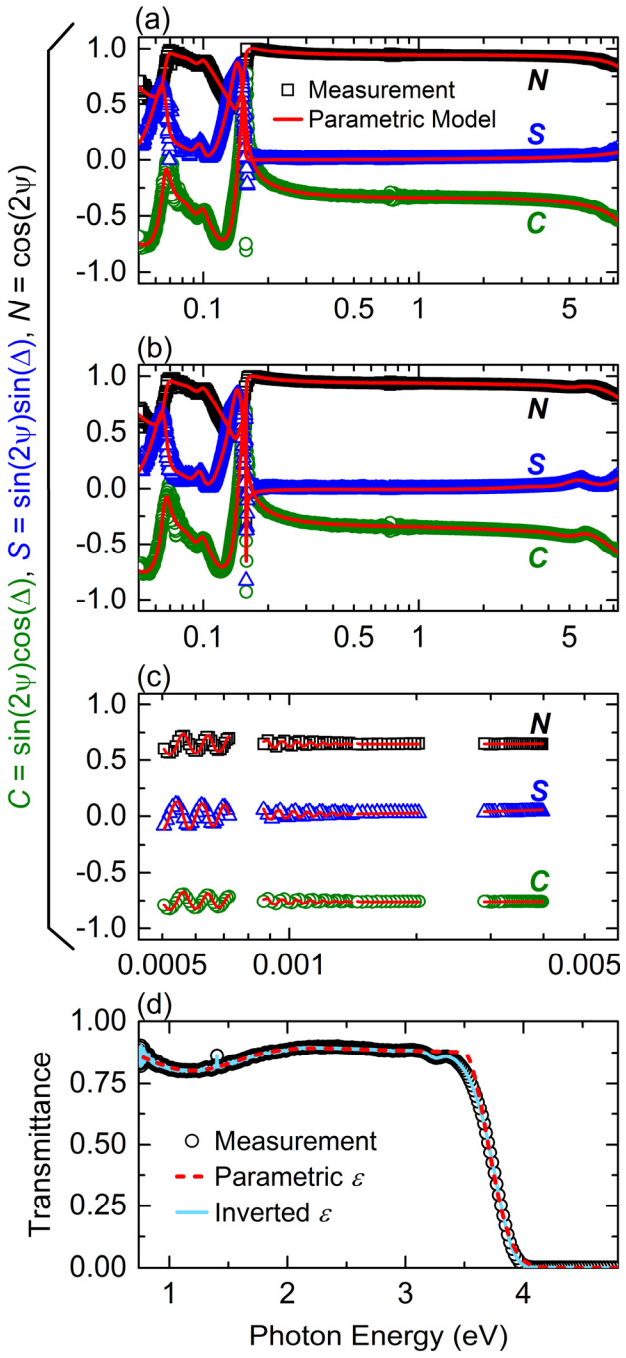

FIG 3. Measured $N = \cos(2\psi)$, $C = \sin(2\psi)\cos\Delta$, $S = \sin(2\psi)\sin\Delta$ spectra and corresponding model simulations for spectroscopic ellipsometry measurements of the (a) air side, (b) tin side, (c) THz spectral range, and measurement of (d) unpolarized transmittance. The red model simulation lines shown in panels (a) – (c) are generated by the parametric models shown in Figure 2 panels (a) – (d), respectively. In panel (d), the red dashed line is generated by fully parametric modeling, whereas the solid cyan line is generated using a numerically inverted ε describing the bulk SLG layer (Accession #01425).

layer is not extended to the THz spectral range because such long wavelengths are not sensitive to that layer and it is therefore not included in the analysis of ellipsometric spectra collected over that wavelength range. Finally, the optical response reported in terms of ε in Figures 4 and 5 can be converted into the complex index of refraction, $N = n + ik$ via $N^2 = \varepsilon$. N describing the bulk SLG layer and tin side layer are shown in Figures 6 and 7, respectively.

The spectral features present in the bulk SLG layer shown in Figures 4 and 6 are detailed in Table I and the sources of the features appearing in the infrared are identified in Table II. This work identifies a phonon absorption at 81 cm^{-1} that, to the best knowledge of the authors, has not previously been reported. Given the fact that this absorption is located in a portion of the spectrum for which there are no measured data points, the low errors associated with these parameters arise from the mathematical description of the quality of fit to the tail regions. The exact nature of this absorption is unclear since it is identified only by its tailing effects into the long-infrared and THz spectral ranges. Si-O-Si and O-Si-O bending modes are identified at both 452.1 ± 0.7 (Refs. 12-16) and 597 ± 8 cm^{-1} (Refs. 14, 15). A Si-O-Si symmetric stretching mode is identified at 767 ± 7 cm^{-1} (Refs. 13, 14, 17, 18). Two anti-symmetric stretching modes are also identified with the transverse mode at 1025.2 ± 0.5 cm^{-1} (Refs. 12, 14, 18) and the longitudinal mode at 1193 ± 2 cm^{-1} (Refs. 12-14, 16, 17). The well-known, broad absorption feature common to all soda lime silicate glasses centered at 8500 cm^{-1} is due to ferrous inclusions[19]. Finally, soda lime glasses are known to have weak ultraviolet absorption bands due to ferric Fe ion inclusions starting at ~2.85 eV with amplitude increasing at higher energies[19]. Although the absorption onset of this glass as modeled by the Tauc-Lorentz oscillator is at 3.49 ± 0.02 eV and at a higher energy than that discussed in Ref. 19, evidence of these weak features resulting in the ultraviolet absorption onset is still visible in the inverted data shown in the insets of Figures 4 and 6. Thus, it is likely that the absorption onset observed in this sample is also resulting from such ferric content.

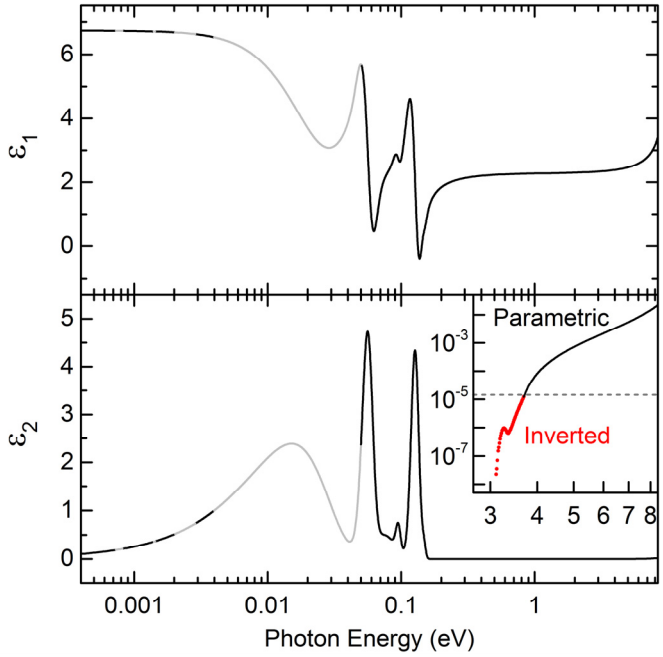

FIG. 4. Spectra in $\varepsilon = \varepsilon_1 + i\varepsilon_2$ describing the bulk soda lime glass layer over the full measured spectral range. The gray lines correspond to spectral regions where there are gaps in the measured spectra. The inset shows ε_2 generated by both parametric modeling and by numerical inversion over ranges of ε_2 where each is most sensitive (Accession #01425).

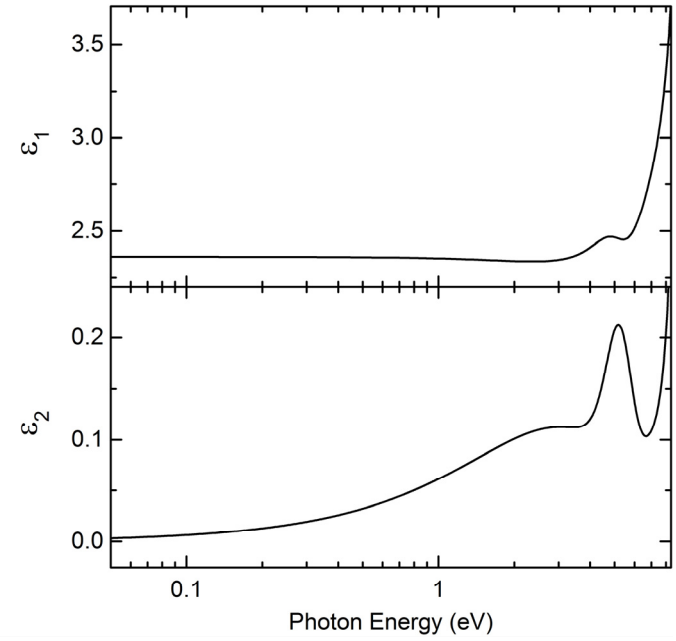

FIG. 5. Spectra in $\varepsilon = \varepsilon_1 + i\varepsilon_2$ describing the tin side layer over a spectral range of 0.05 – 8.37 eV (Accession #01425).

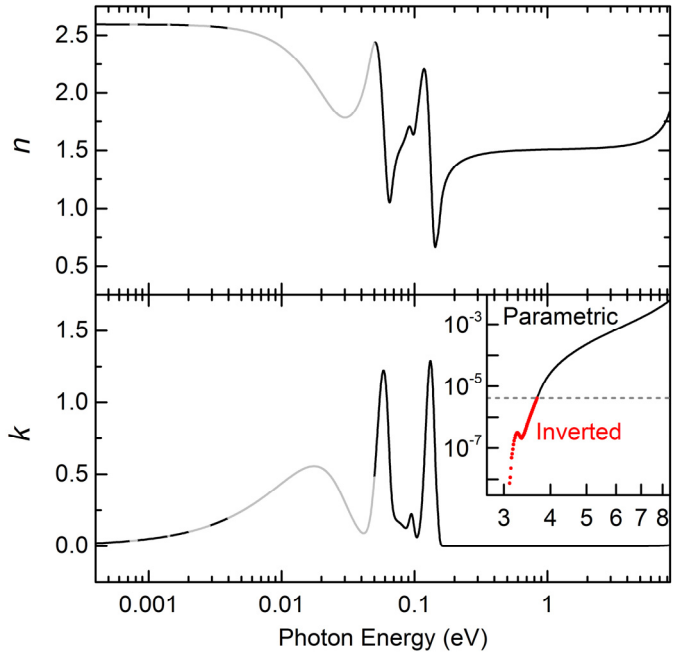

FIG. 6. Spectra in $N = n + ik$ describing the bulk soda lime glass layer over the full measured spectral range. The gray lines correspond to spectral regions where there are gaps in the measured spectra. The inset shows k generated by both parametric modeling and by numerical inversion over ranges of k where each is most sensitive (Accession #01425).

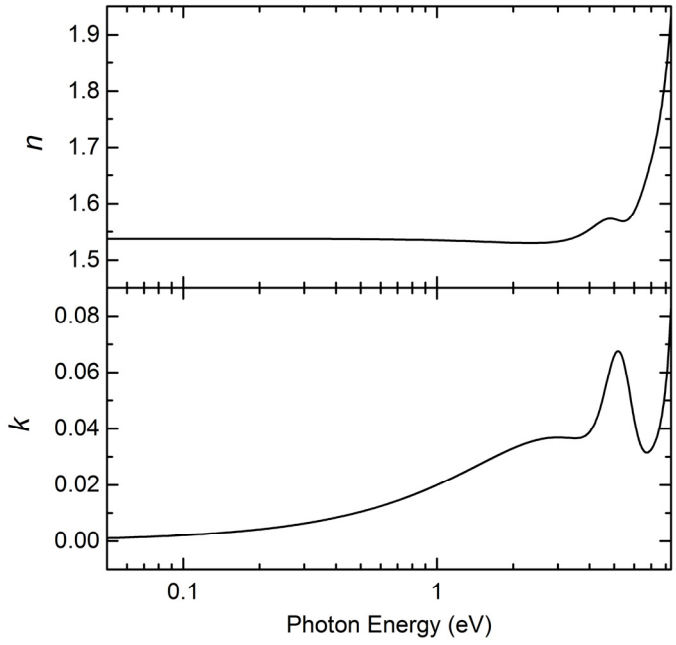

FIG. 7. Spectra in $N = n + ik$ describing the tin side layer over a spectral range of 0.05 – 8.37 eV (Accession #01425).

■ *Oscillator or effective medium approximation equations:*

The equation describing the error function[2] is

$$\sigma = \sqrt{\frac{1}{3W_E - M}\sum_{i=1}^{W_E}\sum_{j=1}^{3}\left(\xi_{i,j}^{mod} - \xi_{i,j}^{exp}\right)^2 + \frac{1}{W_T - M}\sum_{j=1}^{W_T}\left(T_j^{mod} - T_j^{exp}\right)^2}$$

where W_E is the discrete number of measured ellipsometric spectral points, M is the number of free fitting parameters in the models, $\xi_{i,j}$ are the ellipsometric N, C, and S parameters, and W_T is the discrete number of measured T_j^{exp} transmittance spectral points. The equation describing the Lorentz oscillator[3] is

$$\varepsilon_n(E) = \frac{A_n \Gamma_n E_n}{E_n^2 - E^2 - i\Gamma_n E},$$

where A_n, Γ_n, and E_n are the amplitude, broadening, and resonance energy, respectively. The equations describing the imaginary and real parts of the Tauc-Lorentz oscillator[6,7] are

$$\varepsilon_{2_n}(E) = \begin{cases} \left[\frac{A_n E_n \Gamma_n (E - E_{g_n})^2}{E([E^2 - E_n^2]^2 + \Gamma_n^2 E^2)}\right] & , E > E_{g_n} \\ 0 & , E \leq E_{g_n} \end{cases}$$

and

$$\varepsilon_{1_n}(E) = \frac{2}{\pi} P \int_{E_{g_n}}^{\infty} \frac{E' \varepsilon_{2_n}(E')}{E'^2 - E^2} dE' ,$$

where A_n, Γ_n, E_n, E_{g_n}, and P are the amplitude, broadening, resonance energy, Tauc-gap energy, and Cauchy principal value of the Kramers-Kronig integral, respectively. The equations describing the imaginary and real parts of the Gaussian oscillator[4,5] are

$$\varepsilon_{2_n}(E) = A_n e^{-\left(\frac{2\sqrt{\ln(2)}(E-E_n)}{\Gamma_n}\right)^2} - A_n e^{-\left(\frac{2\sqrt{\ln(2)}(E+E_n)}{\Gamma_n}\right)^2}$$

and

$$\varepsilon_{1_n}(E) = \frac{2}{\pi} P \int_{0}^{\infty} \frac{E' \varepsilon_{2_n}(E')}{E'^2 - E^2} dE' ,$$

where A_n, Γ_n, E_n, and P are the amplitude, broadening, resonance energy, and Cauchy principal value of the Kramers-Kronig integral, respectively. The equation describing the Sellmeier oscillator[3] is

$$\varepsilon(E) = \frac{A_n}{E_n^2 - E^2} ,$$

where A_n and E_n are the amplitude and resonance energy, respectively. Finally, the equation describing the Bruggeman effective medium approximation[8,9] is

$$f_a \frac{\varepsilon_a - \varepsilon}{\varepsilon_a + 2\varepsilon} + f_b \frac{\varepsilon_b - \varepsilon}{\varepsilon_b + 2\varepsilon} = 0 ,$$

where the effective optical response of the composite material is obtained by solving for ε and f_a and f_b are the respective volume fractions of the two constituent materials, each with optical response functions ε_a and ε_b, respectively.

Free Parameters in the Model: See Table I below. All parameters listed in Table I are free fitting parameters.

Fixed Parameters in the Model: N/A

Reference Spectra and Sources: N/A

Information Gained From Other Techniques Used to Fix Parameters in the Analysis: N/A

Table of Structure and Optical Properties

TABLE I. All free fitting parameters describing each layer in the analysis models. In cases where no units are listed, the parameter is dimensionless.

			Optical Constants				
Layer	**Material**	**Thickness**	**Expression**	E_n **(eV)**	A_n	Γ_n **(eV)**	E_{g_n} **(eV)**
1	SLG	30 ± 3 Å					
0	SLG	3.12 ± 0.03 mm	Sellmeier	39.8 ± 0.5	1100 ± 200 eV^2	-	-
			Gaussian	0.0100 ± 0.0003	3.2 ± 0.1	0.033 ± 0.002	-
			Gaussian	0.05605 ± 0.00009	4.44 ± 0.08	0.0117 ± 0.0001	-
			Gaussian	0.074 ± 0.001	0.50 ± 0.02	0.038 ± 0.009	-
			Gaussian	0.0951 ± 0.0009	0.5 ± 0.1	0.0092 ± 0.0009	-
			Gaussian	0.12711 ± 0.00006	4.34 ± 0.04	0.0197 ± 0.0002	-
			Gaussian	0.1480 ± 0.0002	0.30 ± 0.01	0.0106 ± 0.0001	-
			Gaussian	1.05 ± 0.03	0.0000110 ± 0.0000005	0.91 ± 0.07	-
			Tauc-Lorentz	10.3 ± 0.7	13 ± 4 eV	0.07 ± 0.01	3.49 ± 0.02
-1	SLG	280 ± 10 Å	Sellmeier	14 ± 7	170 ± 50 eV^2	-	-
			Lorentz	5 ± 3	0.08 ± 0.02	8 ± 12	-
			Gaussian	5.2 ± 0.2	0.12 ± 0.04	1.4 ± 0.5	-
			Lorentz	10 ± 1	7 ± 15	0.5 ± 0.3	-

TABLE II. List of infrared spectral features and their origins as determined by comparison to published literature where available.

Energy (eV)	**Wavenumber (cm^{-1})**	**Origin**
0.0100 ± 0.0003	81 ± 2	
0.05605 ± 0.00009	452.1 ± 0.7	Si-O-Si and O-Si-O bending[12-16]
0.074 ± 0.001	597 ± 8	Si-O-Si and O-Si-O bending[14,15]
0.0951 ± 0.0009	767 ± 7	Si-O-Si symmetric stretching[13,14,17,18]
0.12711 ± 0.00006	1025.2 ± 0.5	Si-O-Si anti-symmetric stretching (transverse)[12,14,18]
0.1480 ± 0.0002	1193 ± 2	Si-O-Si anti-symmetric stretching (longitudinal)[12-14,16,17]
1.05 ± 0.03	8500 ± 200	Ferrous ion inclusions[19]

TABLE III. Spectral features table (Accession #01425).

Spectrum ID #	Identity	Feature or location in range	Photon energy (eV)	Wavelength (μm)	n	k	ε_1	ε_2
01425	Layer -1	Range minimum	0.05	24.80	1.54	0.0011	2.37	0.0033
		Range maximum	8.37	0.148	1.93	0.084	3.74	0.32
01425	Layer 0	Range minimum	0.00041	3024	2.60	0.020	6.73	0.11
		Range maximum	8.37	0.148	1.85	0.0060	3.41	0.022

ACKNOWLEDGMENTS

This work was supported by the University of Toledo start-up funds, Ohio Department of Development Ohio Research Scholar Program (Northwest Ohio Innovators in Thin Film Photovoltaics, Grant No. TECH 09-025), the National Science Foundation (NSF Major Research Instrumentation Program - NSF-MRI Grant. No. 1228917). The authors also thank Pilkington NSG for providing the specimen for measurement.

REFERENCES

[1]Pilkington NSG, *Technical Bulletin: Properties of Soda-Lime Silica Float Glass*, (2013) Retrieved from https://www.pilkington.com/resources/ats129propertiesofglass20130114.pdf.

[2]S. A. Alterovitz and B. Johs, Thin Solid Films **313-314**, 124 (1998).

[3]R. W. Collins and A. S. Ferlauto, *Handbook of Ellipsometry*, edited by H. G. Tompkins and E. A. Irene (William Andrew, Norwich, NY, 2005) pp. 93-235.

[4]K.-E. Peiponen and E. M. Vartiainen, Phys. Rev. B **44**, 8301 (1991).

[5]D. De Sousa Meneses, M. Malki, and P. Echegut, J. Non-Cryst. Solids **352**, 769 (2006).

[6]G. E. Jellison and F. A. Modine, Appl. Phys. Lett. **69**, 371 (1996).

[7]G. E. Jellison and F. A. Modine, Appl. Phys. Lett **69**, 2137 (1996).

[8]D. Aspnes, Thin Solid Films **89**, 249 (1982).

[9]H. Fujiwara, J. Koh, P. I. Rovira, and R. W. Collins, Phys. Rev. B **61**, 10832 (2000).

[10]R. Synowicki, B. D. Johs, and A. C. Martin, Thin Solid Films **519**, 2907 (2011).

[11]W. G. Oldham, Surf. Sci. **16**, 97 (1969).

[12]M. A. Villegas and J. M. Fernandez Navarro, J. Mater. Sci. **23**, 2464 (1988).

[13]A. M. Efimov, J. Non-Cryst. Solids **253**, 95 (1999).

[14]F. H. A. Elbatal, M. M. I. Khalil, N. Nada, and S. A. Desouky, Mat. Chem. Phys. **82**, 375 (2003).

[15]E. M. A. Khalil, F. H. ElBatal, Y. M. Hamdy, H. M. Zidan, M. S. Aziz, and A. M. Abdelghany, Physica B **405**, 1294 (2010).

[16]P. Uprety, M. M. Junda, and N. J. Podraza, Surf. Sci. Spectra **24**, 026003 (2017).

[17]T. A. Sidrov, Appl. Spectrosc. **7**, 376 (1967).

[18]Y.-K. Lee, Y. L. Peng, M. Tomozawa, J. Non-Cryst. Solids **222**, 125 (1997).

[19]C. R. Bamford, *Colour Generation and Control in Glass* (Elsevier Scientific Publishing Company, Amsterdm, The Netherlands, 1977).